ADVANCED ENERGY MATERIALS
www.advenergymat.de

Band Gap Dependence on Cation Disorder in $ZnSnN_2$ Solar Absorber

Tim D. Veal, Nathaniel Feldberg, Nicholas F. Quackenbush, Wojciech M. Linhart, David O. Scanlon, Louis F. J. Piper, and Steven M. Durbin**

Semiconductor material systems with tunable band gaps are of great interest for a variety of optoelectronic applications, including solid state lighting and solar cells. Interest in the Zn-IV-N_2 family of semiconductors has recently increased following the synthesis of the Sn-containing compound, $ZnSnN_2$.[1–5] The Zn-IV-N_2 family of materials has the potential to provide an earth abundant alternative to InGaN and the incumbent thin film photovoltaic absorber materials (such as CdTe and $CuInGaSe_2$) for both light generating and light harvesting technologies. Absorption edges ranging from 2.0 to 3.1 eV have already been demonstrated in Zn(Ge,Sn)N_2 alloys.[6] Even wider spectral coverage from the infrared to the ultraviolet is predicted for Zn(Si,Sn)N_2 alloys.[7] However, an alternative to alloying for tuning the band gap of $ZnSnN_2$ was recently proposed. Hybrid density functional theory (DFT) calculations revealed that altering the degree of cation disorder from none to maximal disorder using the special quasirandom structure (SQS) approach can change the fundamental band gap from 2.09 to 1.12 eV. The possibility of realizing such a variation experimentally was supported by the observation of the cation-disorder-induced wurtzite phase in molecular-beam epitaxy-grown thin films as opposed to the theoretically more stable orthorhombic phase.[3] The cation-ordered orthorhombic structure is a superstructure of wurtzite structure, with similar tetrahedral bonding, as described in ref. [7].

Here, the observed absorption edges as a function of free electron density for the differently grown films are consistent with the room temperature fundamental band gap varying from 1.0 to 2.0 eV as the cation ordering increases. Moreover, the conduction and valence band density of states (DOS) have been calculated using hybrid DFT for the cation-ordered orthorhombic and cation-disordered SQS pseudowurtzite phases. Comparison of these DOS with photoemission data from single crystal $ZnSnN_2$ films grown under different conditions indicates that samples with different degrees of cation ordering have been synthesised, opening up a new method for tuning the band gap of $ZnSnN_2$ films.

The growth conditions for molecular-beam epitaxy (MBE) of the single crystal $ZnSnN_2$ thin films are summarized in **Table 1**. The substrate temperature, the Zn:Sn flux ratio and the N_2 pressure were adjusted to vary the degree of cation disorder in the $ZnSnN_2$ in order to experimentally test the theoretical predictions. X-ray diffraction indicates that all the samples have the wurtzite structure rather than the fully ordered orthorhombic structure (and also that Zn-nitride and Sn-nitride phases are below the detection limit); specifically, the peak at 22° which is characteristic of the orthorhombic structure is absent for all films.[3] Thus, XRD characterization alone is insufficient to exclude the possibility of a significant variation of the degree of cation disorder within the samples grown under the range of conditions employed. Consequently, evidence of cation disorder induced variations in the band gap and band structure has been sought and found in the optical, transport and photoemission properties of the $ZnSnN_2$ films. It is important to note here that in the nonequilibrium growth technique used in this study (plasma-assisted MBE), substrate temperature and flux ratio have a profound influence on adatom migration length, and hence how atoms incorporate into an epitaxially driven structure. Therefore, higher growth temperature is likely to produce a more ordered film than a lower growth temperature. Kinetic processes dominate low temperature MBE as previously observed for the related material $ZnSnP_2$.[8] This is in contrast to close-to-thermodynamic equilibrium growth methods where

Dr. T. D. Veal, Dr. W. M. Linhart
Stephenson Institute for Renewable Energy and Department of Physics
School of Physical Sciences
University of Liverpool
Liverpool L69 7ZF, UK
E-mail: T.Veal@liverpool.ac.uk

N. Feldberg
Department of Physics
University at Buffalo
Buffalo, NY 14260, USA

N. F. Quackenbush, Dr. L. F. J. Piper
Department of Physics
Applied Physics and Astronomy
Binghamton University
Binghamton, NY 13902, USA

Dr. D. O. Scanlon
Kathleen Lonsdale Materials Chemistry
Department of Chemistry
University College London
London WC1H 0AJ, UK

Dr. D. O. Scanlon
Diamond Light Source Ltd.
Diamond House
Harwell Science and Innovation Campus
Didcot, Oxfordshire OX11 0DE, UK

Prof. S. M. Durbin
Department of Electrical and Computer Engineering
Western Michigan University
Kalamazoo, MI 49008, USA
E-mail: durbin@ieee.org

DOI: 10.1002/aenm.201501462

Table 1. Growth conditions and properties of the $ZnSnN_2$ samples.

Sample	Growth temperature [°C]	Zn:Sn flux ratio	N_2 pressure [Torr]	Optical gap [eV]	Free electron density, n [cm^{-3}]
P35	400	39	2×10^{-5}	1.33	2.7×10^{20}
P36	400	36	2×10^{-5}	2.12	1.1×10^{21}
P50	400	36	1×10^{-5}	2.38	3.0×10^{20}
P64	500	55	1×10^{-5}	2.18	1.4×10^{19}
P65	450	55	1×10^{-5}	2.21	1.2×10^{20}

thermodynamics dominates and the more disordered structure is expected at higher growth temperature. The energy difference between the cation-ordered and cation-disordered structures is 0.09 eV per atom. Using the regular solution approximation to Gibbs free energy, the temperature for the transition from order to maximal disorder is found to be 1209 °C.

The optical absorption data from $ZnSnN_2$ samples grown under the different conditions are shown in **Figure 1**. The absorption onsets vary between 1.33 and 2.38 eV. The absorption coefficient, α, rapidly increases to 5×10^4 cm^{-1} (2.5×10^9 cm^{-2} for α^2) above each onset, a value typical of direct band gap semiconductors. The plot of α^2 versus photon energy exhibits approximately linear behaviour, again consistent with a direct band gap. The features below the sharp onset are due to Fabry–Perot oscillations associated with the 120–165 nm thickness of the $ZnSnN_2$ films. The free electron densities of the samples, determined by Hall effect measurements, were found to vary between 1.3×10^{19} and 1.1×10^{21} cm^{-3}. The measured electron mobility was in the range 7–12 cm^2 V^{-1} s^{-1} for all samples. The free electron density did not vary with temperature, indicating the presence of unintentional degenerate n-type doping. The absorption spectra are therefore expected to be influenced by conduction band filling, the well-known Burstein–Moss effect.[9,10] That is, transitions between the band extrema do not occur—only direct transitions from the valence band to the states at or above the Fermi level within the conduction band contribute to the absorption spectra.

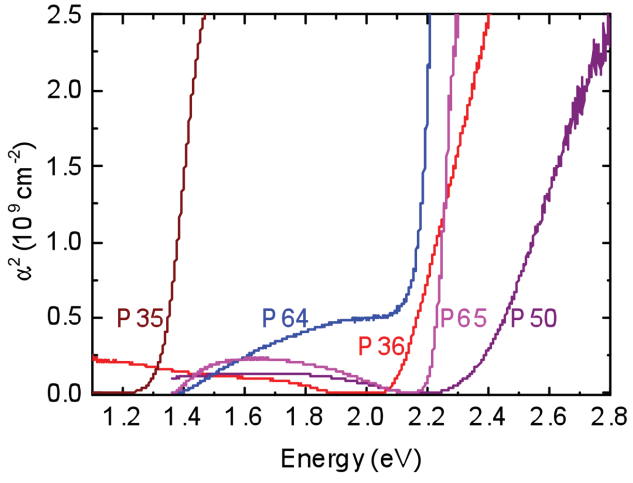

Figure 1. Optical absorption spectra from $ZnSnN_2$ films grown under different conditions as detailed in Table 1.

The energy of the optical absorption edge of each film is plotted against the corresponding free electron density in **Figure 2**a. It is immediately apparent that there is no simple trend of Burstein–Moss shift whereby the absorption onset increases as the free electron density increases. Therefore, these data points are compared with the Burstein–Moss shift expected for the calculated band structures of ordered and SQS disordered $ZnSnN_2$. The DFT band structure for these two extremes in the vicinity of the Γ point are shown in Figure 2b. At the Γ point, the band gap is 2.18 eV for the cation ordered othorhombic structure and 1.12 eV for the SQS cation disordered pseudowurtzite structure. The DFT bands were fitted using a nonparabolic $\boldsymbol{k \cdot P}$ conduction band dispersion and parabolic valence bands; these are shown by the lines in Figure 2b. This fitting was used to determine the conduction band edge effective masses from the DFT. For the orthorhombic structure, the electron-effective masses are 0.10, 0.15, and $0.21m_0$ in the three different directions, giving a geometric mean value of $0.147m_0$ to be used in the calculations of optical gap versus free electron density. For the SQS disorderd pseudowurtzite structure, the electron effective mass is isotropic and is $0.12m_0$. These effective masses were then used with the DFT band gaps, reduced by ≈0.15 eV to account for room temperature, to generate a numerical conduction band density of states, incorporating conduction band nonparabolicity and band gap renormalization.[11] This was in turn used to calculate the Fermi level position with respect to the conduction band minimum as a function of free electron density for the cation ordered orthorhombic and SQS disordered pseudowurtzite structures. The Fermi level position combined with the valence band dispersion enabled the optical gap to be determined as a function of free electron density.

The results are shown for the two extreme cases of cation ordered and SQS cation disordered $ZnSnN_2$ in Figure 2a. The experimental data points on the figure fall close to the line for SQS cation disorder for samples grown under the most nitrogen-rich conditions. For the samples grown with the metal to nitrogen ratio increased by a factor of two, the data points lie between the lines corresponding to cation ordered orthorhombic and SQS disordered wurtzite. This is consistent with the X-ray diffraction results that show all samples are wurtzite; the peak at 22° characteristic of the orthorhombic structure $ZnSnN_2$ is absent for all films. It also suggests that the degree of cation disorder is less in the samples grown under more metal-rich conditions. This is expected as metal-rich conditions are likely to lead to higher quality growth of $ZnSnN_2$, as in the case of conventional III-nitrides.[12] Among these samples grown under more metal-rich conditions, increasing the Zn:Sn ratio and the growth temperature leads to a lower carrier density and data points lying closer to the line calculated for cation ordered $ZnSnN_2$. A higher Zn:Sn ratio is likely to lead to fewer unintentional donors (such as Sn_{Zn} antisites[13] related to excess Sn owing to the relatively high vapor pressure of zinc; this is also seen for the samples grown under less metal-rich conditions. As mentioned earlier, for low temperature MBE growth, higher growth temperature is expected to give a higher degree of cation ordering and a structure closer to that which is the most thermodynamically stable.

Taken together, the optical and DFT results imply that varying the growth conditions of $ZnSnN_2$ can alter the fundamental band gap by more than 1 eV by changing the degree of cation disorder. This is seen most clearly by comparing the two

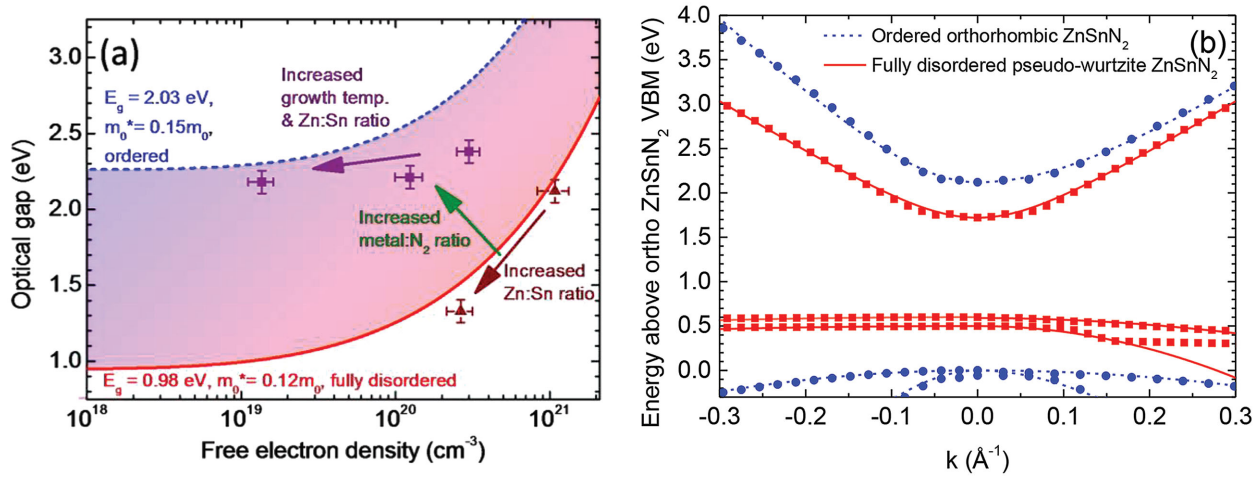

Figure 2. a) Optical absorption edge versus free electron density for the $ZnSnN_2$ films. The calculated dependence of absorption on free electron density is also shown for the two extreme cases of cation ordered (blue dashed line) and fully cation disordered (red solid line) $ZnSnN_2$. The calculations are performed using ***k·P*** band structures fitted to the DFT results close to the Γ point. The square points correspond to samples grown under less metal-rich conditions and triangular points to those grown under more metal-rich conditions. b) DFT band structure (points) and ***k·P*** fitting for cation ordered orthorhombic (blue solid lines) and SQS cation disordered pseudowurtzite (red dashed lines) $ZnSnN_2$.

samples with $n \approx 3 \times 10^{20}$ cm^{-3}, P35 and P50, which have absorption edges of 1.33 and 2.38 eV, respectively.

A few previous experimental studies of the optical properties of $ZnSnN_2$ have been reported by other groups.[2,4] Lahourcade et al. reported experimental optical gaps of 1.9 and 2.2 eV for sputtered polycrystalline $ZnSnN_2$ with electron concentrations as high as 10^{21} cm^{-3}. The X-ray diffraction data from this material was interpreted as indicating orthorhombic structure. The optical gap values were suggested to be consistent with Burstein–Moss shift and a DFT-calculated fundamental band gap of 1.42 eV for the orthorhombic material obtained using the HSE06 functional with $\alpha = 0.25$, that is, 25% of the semilocal generalized gradient approximation exchange potential replaced by screened Fock exchange. This DFT $ZnSnN_2$ band gap contrasts with the ≈2 eV values obtained using PBE0 and GW,[3,7] and the value of 1.84 eV obtained with HSE06 and $\alpha = 0.31$.[13] Quayle et al., meanwhile, reported from wurtzite $ZnSnN_2$ a broad photoluminescence peak between 1.4 and 1.6 eV and suggested the band gap is 1.7 eV from photoluminescence excitation spectroscopy.[4,14] However, the carrier concentration was not reported due to the films being supported by a Zn–Sn alloy, preventing meaningful Hall effect results from the $ZnSnN_2$ films. Recently, there have been two separate reports of sputtered polycrystalline thin films exhibiting lower carrier densities.[15,16] Deng et al. reported electron concentrations between 2.3×10^{17} and 1.6×10^{18} cm^{-3} with band gaps estimated in the range 1.82 to 1.95 eV, but with significant absorption above 1.4 eV.[15] Fioretti et al. reported carrier densities between 1.8×10^{18} and $\approx 4.5 \times 10^{20}$ cm^{-3} with the highest mobility being 8 cm^2 V^{-1} s^{-1}. The lowest carrier densities are for Zn-rich films and with stoichiometric films all having free electron density of greater than 10^{20} cm^{-3}. Absorption onsets for these films were between 1.0 and 1.4 eV with the lowest carrier density films all having their absorption edge close to 1.0 eV.[16] All of the experimental results reported so far can, therefore, be interpreted in terms of the presence of cation disorder, a fundamental band gap varying with decreasing disorder from 1.0 to 2.0 eV and Burstein–Moss shift.

In order to investigate further the cation disorder in the MBE-grown films, hard X-ray photoemission spectroscopy (HAXPES) has been used to measure the valence band spectra of the $ZnSnN_2$ samples grown under different conditions to compare them to the valence band density of states calculated by DFT for the cation ordered orthorhombic and SQS disordered

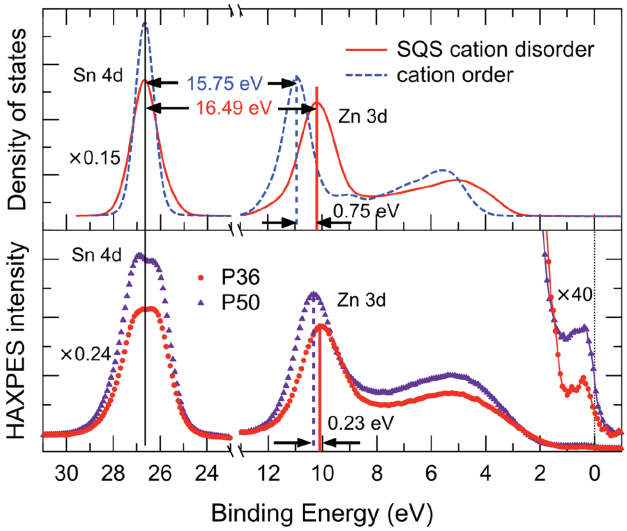

Figure 3. Valence band and shallow core level HAXPES data from two different $ZnSnN_2$ films, compared with hybrid DFT broadened density of states (DOS) for the cation-ordered orthorhombic structure (dashed line) and the SQS cation disordered pseudowurtzite structure (solid line). The zero of the binding energy scale corresponds to the Fermi edge of both samples; the calculated DOS are then aligned by setting the centre of Sn 4d peak to the same energy as for P50. The DOS intensity scale is the same for both the ordered and SQS cation disordered cases and the HAXPES is scaled so that the background intensity is the same for both spectra.

pseudowurtzite structures. The use of HAXPES circumvents issues associated with surface preparation required for traditional XPS, because of the combination of increased attenuation length and reduced sensitivity to adventitious carbon, and oxygen species. As a result, the carrier concentrations of the measured films were not modified by in-vacuum annealing or sputtering.[17]

The HAXPES data for the valence band and shallow core levels are shown in **Figure 3** for two samples grown under identical conditions except that one was grown under less metal-rich conditions (P36) and one was grown under more metal-rich conditions (P50). The DFT calculated densities of states are also shown after cross section correction,[18] and after broadening (see the Experimental Section). The different Sn 4d to Zn 3d separations in the calculated spectra are characteristic of the extremes of cation disorder, from the cation ordered orthorhombic structure with the smallest separation (15.75 eV) to the higher separation (16.49 eV) for the wurtzite structure with SQS cation disorder. By comparison with the calculated spectra, the sample grown under less metal-rich conditions (P36) has a greater degree of cation disorder than the one grown under more metal-rich conditions (P50). The experimental curves were aligned using the Fermi edge emission from the $ZnSnN_2$ films. The calculated DOS were in turn aligned by setting their Sn 4d semicore level energy for all calculated spectra to the value of 26.67 eV found for both P36 and P50, enabling direct comparison between the experimental spectra and the calculated DOS. In Figure 3, good agreement is apparent in terms of spectral shape and peak energies between P36 and the calculated DOS for the SQS disordered pseudowurtzite phase. The Zn 3d semicore level of P50, meanwhile, lies between the DFT calculated endpoints of SQS cation disorder and completely cation ordered, consistent with P50 being less disordered than P36, as expected for more metal-rich growth conditions. These particular results should be viewed in the context of DFT generally not being very good for calculating the correct energies of semicore levels. However, the method used here, the PBE0 approach, is known to give better results than standard DFT.

The degenerate nature of the films means that, in addition to the valence band, some conduction band states are also occupied and are apparent in the HAXPES spectra with a Fermi edge and low intensity conduction band emission feature. This enables HAXPES to be used to confirm the difference in optical gap between these two films—the Fermi edge to valence band onset separation is ≈2.15 eV for P50 and ≈1.90 eV for P36. The difference between these two values of 0.25 eV is comparable with the difference of 0.26 eV between optical gaps determined from absorption data for these samples. The Fermi edge to valence band onset values are about 0.2 eV lower than the optical gaps as they represent the valence band maximum to Fermi level separation as opposed to the direct transition seen in optical data at the Fermi wavevector from slightly lower in the valence band to the Fermi level.

In conclusion, the earth abundant element semiconductor $ZnSnN_2$ has been grown by molecular-beam epitaxy with various substrate temperatures, Zn:Sn ratios and metal:nitrogen ratios. All the samples have the wurtzite structure as opposed to the expected most thermodynamically stable orthorhombic structure. Density functional theory calculations of the band structure of cation ordered orthorhombic and fully cation disordered pseudowurtzite $ZnSnN_2$ have enabled $\boldsymbol{k \cdot P}$ parameters to be determined for each of these cases. This in turn allowed the variation of the optical gap with free electron density to be calculated for the two extremes of cation disorder, including the effects of conduction band non-parabolicity and band gap renormalization. The optical gaps determined from absorption spectroscopy (1.33–2.38 eV) and the free electron densities from Hall effect data (1.4×10^{19} to 1.1×10^{21} cm^{-3}) fall between the curves calculated for these extreme cases and the inferred degree of cation disorder correlates with the growth conditions. Comparison of HAXPES valence band spectra from two samples grown under different conditions with DFT-calculated valence band DOS for ordered orthorhombic and fully disordered pseudowurtzite $ZnSnN_2$ provides further evidence of differing degrees of cation disorder in the $ZnSnN_2$ samples. These results indicate that the fundamental band gap of $ZnSnN_2$ can be varied between 1.0 and 2.0 eV by tuning the degree of cation disorder by varying the growth conditions, precluding the need for alloying. This suggests $ZnSnN_2$ has potential as an earth abundant semiconductor for solar cells and other optoelectronics. Further work to reduce the free electron density and also to develop intentional n- and p-type doping is required for applications of this promising material. This methodology of varying the band gap by tuning the degree of cation disorder is applicable to other heterovalent ternary semiconductors.

Experimental Section

Molecular-Beam Epitaxy: Single crystal $ZnSnN_2$ films were grown by *N*-plasma-assisted molecular-beam epitaxy on yttria-stabilized cubic zirconia (111) substrates broadly as described in refs. [3] and [5]. The film thicknesses were in the range 120–165 nm as determined by cross-sectional scanning electron microscopy. The substrate temperatures, N_2 pressures and nominal Zn:Sn flux ratios, as determined by quartz crystal micro balance, used for the growth of the different films are shown in Table 1. All films grown with an appropriate overpressure of Zn (which must be increased when increasing the substrate temperature) exhibit stoichiometric Zn to Sn ratio, within the accuracy of the Rutherford backscattering spectrometry employed.

Optical Absorption and Hall Effect: Near-infrared and visible reflectance and transmittance measurements at an incident angle of 11° relative to the surface normal were performed at room temperature using a Bruker Vertex 70V Fourier-transform infrared (FTIR)/visible spectrometer using a tungsten lamp, a Si diode detector, and a quartz beamsplitter. The transmittance and reflectance spectra were used to calculate the absorption coefficient. Hall effect measurements were performed between 25 and 300 K in the Van der Pauw configuration with a 0.8 T magnetic field using a Semimetrics system.

HAXPES: The HAXPES measurements were performed at the National Institute of Standards and Technology (NIST) bending magnet beamline X24 at the National Synchrotron Light Source (NSLS) at Brookhaven National Laboratory. Measurements were performed using a photon energy $h\nu$ = 4000 eV, with a pass energy of 500 eV, with a Gaussian instrumental broadening of 0.5 eV. The binding energy axis was referenced to the Au $4f_{7/2}$ peak and Fermi edge of the Au foil in contact with the film. The emission angle was set to 85° to the surface plane to increase the bulk sensitivity.

Band structure calculations were performed using the periodic DFT code VASP[19,20] in which a plane-wave basis set describes the valence electronic states. The Perdew–Burke–Ernzerhof (PBE) gradient corrected functional was used to treat the exchange and correlation.[21] The projector augmented wave method was used to describe the

interactions between the cores (Zn:[Ar], Sn:[Kr], and N:[He]) and the valence electrons,[22,23] so that the Zn 3d and Sn 4d states were explicitly included. In this study, we have employed the hybrid density functional PBE0 developed by Adamo and Barone[24] as implemented in the VASP code.[25] To simulate the cation disordered system, a 72 atom super cell was generated using the special quasirandom structures (SQS) approach,[26] in which the most relevant atom-atom correlations of the cations approach that of a random alloy. In detail, the 36 N atoms in the 72-atom SQS supercell have the following nearest neighbour configurations: 1 bonded to 4 Zn atoms, 1 bonded to 4 Sn atoms, 11 bonded to 3 Zn, and 1 Sn atoms, 12 bonded to 2 Zn, and 2 Sn atoms, and 11 bonded to 1 Zn, and 3 Sn atoms. For comparison with the experimental HAXPES data, the calculated the partial densities of states have been weighted by their orbital cross-sections for $h\nu = 4000$ eV, and after convolution with Lorentzian and Gaussian lineshapes to reflect the lifetime broadening (0.1 eV) and the instrumental broadening of the photoemission system (0.5 eV).

Acknowledgements

Work at UB and UWM was supported by National Science Foundation (NSF) Grant No. DMR-1410915 and DMR-1244887(Program Manager Charles Ying) and at UL by EPSRC Grant No. EP/G004447/2. L.F.J.P. and N.F.Q. acknowledge support from the NSF under Grant No. DMR-1409912. D.O.S. acknowledges the use of the ARCHER supercomputer via membership of the Materials Chemistry Consortium, funded by EPSRC Grant No. EP/L000202/1. D.O.S. and T.D.V. acknowledge membership of the Materials Design Network. The authors thank Barry Karlin and Joe Woicik for use of the X24a NIST HAXPES end station at the NSLS. The NSLS is supported by the U.S. Department of Energy under Contract No. DE-AC02-98CH10886.

Received: July 21, 2015
Revised: August 27, 2015
Published online:

[1] N. Feldberg, B. Keen, J. D. Aldous, D. O. Scanlon, P. A. Stampe, R. J. Kennedy, R. J. Reeves, T. D. Veal, S. M. Durbin, presented at *Proc. 38th IEEE Photovoltaic Specialists Conf. (PVSC)*, Austin, Texas, USA, June **2012**, p. 2524.
[2] L. Lahourcade, N. C. Coronel, K. T. Delaney, S. K. Shukla, N. A. Spaldin, H. A. Atwater, *Adv. Mater.* **2013**, *25*, 2562.
[3] N. Feldberg, J. D. Aldous, W. M. Linhart, L. J. Phillips, K. Durose, P. A. Stampe, R. J. Kennedy, D. O. Scanlon, G. Vardar, R. L. Field III, T. Y. Jen, R. S. Goldman, T. D. Veal, S. M. Durbin, *Appl. Phys. Lett.* **2013**, *103*, 042109.
[4] P. C. Quayle, K. Hea, J. Shana, K. Kash, *MRS Commun.* **2013**, *3*, 135.
[5] N. Feldberg, J. D. Aldous, P. A. Stampe, R. J. Kennedy, T. D. Veal, S. M. Durbin, *J. Electron. Mater.* **2014**, *43*, 884.
[6] P. Narang, S. Chen, N. C. Coronel, S. Gul, J. Yano, L-W. Wang, N. S. Lewis, H. A. Atwater, *Adv. Mater.* **2014**, *26*, 1235.
[7] A. Punya, W. R. L. Lambrecht, M. van Schilfgaarde, *Phys. Rev. B* **2011**, *84*, 165204.
[8] S. Francoeur, G. A. Seryogin, S. A. Nikishin, H. Temkin, *Appl. Phys. Lett.* **2000**, *76*, 2017.
[9] E. Burstein, *Phys. Rev.* **1954**, *93*, 632.
[10] T. S. Moss, *Proc. Phys. Soc. London Sec. B* **1954**, *67*, 775.
[11] J. Wu, W. Walukiewicz, W. Shan, K. M. Yu, J. W. AgerIII, E. E. Haller, Hai Lu, W. J. Schaff, *Phys. Rev. B* **2002**, *66*, 201403.
[12] W. E. Hoke, A. Torabi, J. J. Mosca, T. D. Kennedy, *J. Vac. Sci. Technol. B* **2007**, *25*, 978, and references therein.
[13] S. Chen, P. Narang, H. A. Atwater, L-W. Wang, *Adv. Mater.* **2013**, *26*, 311.
[14] P. C. Quayle, E. W. Blanton, A. Punya, G. T. Junno, K. He, L. Han, H. Zhao, J. Shan, W. R. L. Lambrecht, K. Kash, *Phys. Rev. B* **2015**, *91*, 205207.
[15] F. Deng, H. Cao, L. Liang, J. Li, J. Gao, H. Zhang, R. Qin, C. Liu, *Optics Lett.* **2015**, *40*, 1282.
[16] A. N. Fioretti, A. Zakutayev, H. Moutinho, C. Melamed, J. D. Perkins, A. Norman, M. Al-Jassim, E. Toberer, A. C. Tamboli, *J. Mater. Chem. C*, **2015**, DOI: 10.1039/C5TC02663F.
[17] J. J. Mudd, Tien-Lin Lee, V. Muñoz-Sanjosé, J. Zuñiga-Pérez, D. Hesp, J. M. Kahk, D. J. Payne, R. G. Egdell, C. F. McConville, *Phys. Rev. B* **2014**, *89*, 035203.
[18] J. H. Scofield, *Lawrence Livermore National Laboratory Report No. UCRL-51326* **1973**.
[19] G. Kresse, J. Furthmüller, *Phys. Rev. B* **1996**, *54*, 11169.
[20] G. Kresse, J. Hafner, *Phys. Rev. B* **1994**, *49*, 14251.
[21] J. P. Perdew, K. Burke, M. Ernzerhof, *Phys. Rev. Lett.* **1996**, *77*, 3865.
[22] P. E. Blöchl, *Phys. Rev. B* **1994**, *50*, 17953.
[23] G. Kresse, D. Joubert, *Phys. Rev. B* **1999**, *59*, 1758.
[24] C. Adamo, V. Barone, *J. Chem. Phys.* **1999**, *110*, 6158.
[25] J. Paier, M. Marsman, K. Hummer, G. Kresse, I. C. Gerber, J. G. Angyan, *J. Chem. Phys.* **2006**, *124*, 154709.
[26] A. Zunger, S. H. Wei, L. G. Ferreira, J. E. Bernard, *Phys. Rev. Lett.* **1990**, *65*, 353.

